JOURNAL OF MATERIALS SCIENCE 30 (1995) 5600–5606

Effect of hydrothermal synthesis environment on the particle morphology, chemistry and magnetic properties of barium hexaferrite

A. ATAIE*, M. R. PIRAMOON†, I. R. HARRIS*, C. B. PONTON*‡
** School of Metallurgy and Materials, and ‡ IRC in Materials for High Performance Applications, The University of Birmingham, Edgbaston, Birmingham, B15 2TT, UK*

Barium nitrate and iron nitrate have been used as precursors in the hydrothermal synthesis of barium hydroxide, iron oxide and barium hexaferrite sols under specified standard synthesis conditions (temperature, time, stirring, alkali concentration, amount of water and heating rate) as a function of the base species used during synthesis. The hydrothermal synthesis of barium hydroxide and iron oxide has been used to develop an understanding of the hydrothermal synthesis of barium hexaferrite from a mixture of their precursors. The investigation has shown that the nucleation and growth behaviour as well as the phase composition, thermal behaviour, particle size, particle-size distribution and magnetic properties are strong functions of the base species used. The electrostatic potential difference between the barium hydroxide and the iron oxide decreases with increasing cation size in the order NaOH, KOH, $(C_2H_5)_4NOH$ and NH_4OH. Note the potential difference between the two sol species determines their tendency to coagulate into clusters; hence, the heterocoagulation will be greater when using NaOH or KOH than $(C_2H_5)_4NOH$ or NH_4OH. Under the standard synthesis conditions, only NaOH and KOH are able to facilitate the formation of plate-like particles of barium hexaferrite. In contrast, ultrafine particles of iron oxide (10–20 nm) together with only a small amount of barium hexaferrite are produced when either NH_4OH or $(C_2H_5)_4NOH$ base is used. The samples synthesized in the presence of the NaOH and KOH exhibit relatively higher saturation magnetization (i.e. 258 mT (39 e.m.u. g^{-1}) and 215 mT (32 e.m.u. g^{-1}), respectively) than those samples synthesized in the presence of NH_4OH or $(C_2H_5)_4NOH$ which exhibit negligible saturation magnetization owing to the small amount of magnetic phase ($BaFe_{12}O_{19}$) present.

1. Introduction

In addition to permanent magnet applications, barium hexaferrite ($BaFe_{12}O_{19}$) powder with its excellent chemical stability is a promising material for perpendicular high-density recording media [1, 2]. The powder needs to be ultrafine with a narrow size distribution, comprising hexagonal plate-like particles of barium hexaferrite with good dispersivity. Such particles cannot be produced easily and routinely by the conventional mixed oxide ceramic method (which involves the calcination of a mixture of $BaCO_3$ and αFe_2O_3 at around 1200 °C); thus, a process other than the conventional route is needed.

Wet chemical methods, such as coprecipitation [1, 2], organometallic precursor [3, 4], citrate precursor [5, 6] and hydrothermal methods are nowadays being developed for the synthesis of ultrafine particles of barium hexaferrite. The use of hydrothermal processing to synthesize pure, ultrafine, stress-free barium hexaferrite powder with a narrow size distribution at a relatively low temperature (200–300 °C) appears to have attracted much attention in recent years [7–14]. Although the hydrothermal synthesis of barium hexaferrite particles from different precursors (i.e $Ba(NO_3)_2$ and $Fe(NO_3)_3 \cdot 9H_2O$ mixtures in the presence of NaOH [7, 9, 12]; FeOOH and $Ba(OH)_2$ mixture [7, 8, 11–13]; αFe_2O_3 and $Ba(OH)_2$ mixtures [7, 10, 13]; and $FeCl_3$ and $Ba(OH)_2$ mixtures [14]) and the effect of the synthesis conditions on the morphology of the product particles, have both been investigated earlier, the synthesis of barium hexaferrite from nitrate precursors in the presence of various base species, other than NaOH, has not yet been investigated. In addition, the magnetic properties of barium hexaferrite particles synthesized hydrothermally from nitrate precursors have not been measured.

The objective of the present investigation was to gain an understanding of the role of the inorganic and organic bases in the formation of barium hexaferrite from nitrate precursors by hydrothermal processing. In order to achieve this aim, various sols were synthesized hydrothermally under the same synthesis conditions but using different base species; the effects of the base species and the sol solution pH on the

0022–2461

TABLE I Molar amounts of the starting precursor(s) and base used for the different sample mixtures processed under the standard synthesis conditions

Sample	Precursor(s)	Molar amount	Base	Molar amount
BN1	Barium nitrate	0.015	NaOH	0.06
BN2	Barium nitrate	0.015	KOH	0.06
BN3	Barium nitrate	0.015	NH_4OH	0.06
BN4	Barium nitrate	0.015	TEAH[a]	0.06
IN1	Iron nitrate	0.015	NaOH	0.09
IN2	Iron nitrate	0.015	KOH	0.09
IN3	Iron nitrate	0.015	NH_4OH	0.09
IN4	Iron nitrate	0.015	TEAH	0.09
IB1	Barium and Iron nitrates	0.00375 0.03	NaOH	0.195
IB2	Barium and Iron nitrates	0.00375 0.03	KOH	0.195
IB3	Barium and Iron nitrates	0.00375 0.03	HN_4OH	0.195
IB4	Barium and Iron nitrates	0.00375 0.03	TEAH	0.195

[a] tetraethyl ammonium hydroxide.

particle characteristics were then investigated in a systematic manner.

2. Experimental procedure

Iron nitrate [$Fe(NO_3)_3 \cdot 9H_2O$] and barium nitrate [$Ba(NO_3)_2$] precursors (Aldrich Ltd), were used in the hydrothermal synthesis of barium hydroxide, iron oxide and barium hexaferrite, for which a 250 ml capacity, PTFE-lined, Berghof laboratory autoclave was employed. The hydrothermal processing of the individual precursors to produce barium hydroxide and iron oxide was done in order to compare and contrast it with the simultaneous hydrothermal decomposition of these precursors to produce barium hexaferrite. Sodium hydroxide (NaOH), potassium hydroxide (KOH), ammonium hydroxide (NH_4OH) and tetraethyl ammonium hydroxide [$(C_2H_5)_4NOH$] were used as the base species for the hydrothermal synthesis in the expectation of their acting as base catalysts.

Aqueous solutions of the precursors plus base species were prepared with a OH^-/NO_3^- molar ratio of 2 and subsequently synthesized hydrothermally by heating at about 5 °C min^{-1} to 220 °C and holding for 5 h without stirring. These synthesis conditions are hereafter referred to as standard synthesis conditions. The synthesized sols were washed with distilled water and then dried at room temperature. Table I gives the molar amounts of precursor(s) and base used for the 12 sample mixtures which were hydrothermally processed in this work.

Powder particle-phase identification was made by X-ray powder diffraction (XRD, CuK_α radiation). The particle morphology was studied by SEM, TEM, while particle-size distribution was determined by laser diffraction particle-size analysis (Coulter LS 130). The thermal and magnetic behaviour was evaluated by simultaneous thermogravimetric/differential thermal analysis (TG/DTA) and by a vibrating sample magnetometer (VSM), respectively. The DTA/TG results were correlated with the XRD analysis; calcined, high-purity α-alumina was used as the TG/DTA reference sample. A Delsa 440 was used to measure the surface charge mobility of the sol particles.

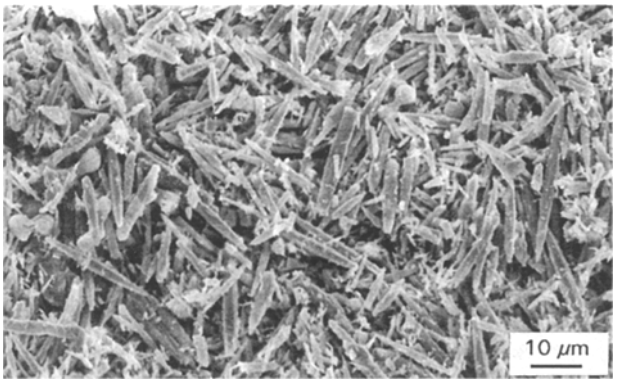

Figure 1 Scanning electron micrograph of the product (barium hydroxide) from the hydrothermal processing of the barium nitrate–NH_4OH (aq) mixture under the standard synthesis conditions.

3. Results and discussion

3.1. Hydrothermal processing of barium and iron nitrates in isolation

Analysis of the powder X-Ray diffraction patterns and the scanning electron micrographs of the products synthesized hydrothermally from the barium nitrate precursor under the standard synthesis conditions, using different base species, indicates the formation of needle-like particles of mainly barium hydroxide [$\alpha Ba(OH)_2$] with correspondingly different particle sizes and size distributions. Fig. 1 shows a scanning electron micrograph of barium hydroxide synthesized using NH_4OH as the base (BN3). The presence of some spherical particles can be attributed to BaO with a cubic structure.

Given the needle-like and agglomerated nature of the particles, the laser diffraction size analysis results do not give a true particle size but rather an agglomerate size, i.e. effective particle cluster size. The mean particle length as determined by SEM image analysis together with the mean, modal and 95% confidence limits particle sizes from the Coulter LS 130, are tabulated in Table II.

The powder X-ray diffraction patterns and the scanning electron micrographs of the products from the hydrothermal processing of iron nitrate under the standard synthesis conditions using different base species, both confirm the formation of hexagonal plate-like particles of iron oxide (αFe_2O_3) with correspondingly different particle sizes and size distributions. Fig. 3 shows a scanning electron micrograph of hexagonal particles of αFe_2O_3 with an average particle-face size of 0.5 μm, produced under the standard synthesis conditions from a mixture of iron nitrate and NaOH (aq). The hydrothermal synthesis of fine, plate-like particles of αFe_2O_3, with a size of 1–2 μm, from a mixture of iron nitrate and NaOH (aq) at 300 °C for 5 h has been reported earlier [9], supporting the current results;

TABLE II Particle shape, mean particle length (determined by SEM) and mean, modal and 95% confidence limits particle sizes (from Coulter LS 130) of the products from the hydrothermal processing of the barium nitrate under the standard synthesis conditions as a function of base species

Sample	Base	Shape of the particles	Mean length (μm) SEM	Mean size (μm) LS 130	Mode (μm) LS 130	95% Conf. limits (μm) LS 130
BN1	NaOH	Needle-like	3.5	56.68	88.29	46.23–67.14
BN2	KOH	Needle-like	5.0	176.3	219	140.9–211.7
BN3	NH_4OH	Needle-like	13.0	24.1	22.53	19.41–28.86
BN4	$(C_2H_5)_4NOH$	Needle-like	10.5	118.5	219.4	96.47–140.6

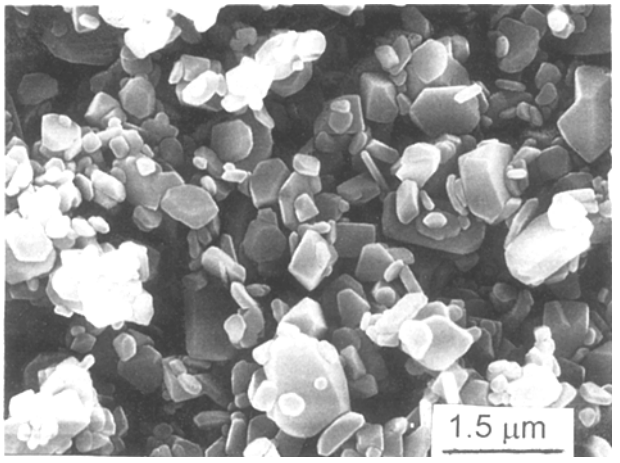

Figure 2 Scanning electron micrograph of the product (iron oxide) from the hydrothermal processing of the iron nitrate–NaOH (aq) mixture under the standard synthesis conditions.

however, the average particle size of the iron oxide formed in the present work is significantly smaller than 1 μm, which is a probable consequence of the lower synthesis temperature of 220 °C.

The mean particle diameter as determined by SEM image analysis, together with the mean, modal and 95% confidence limits particle sizes from the Coulter LS 130, of iron oxide as a function of base species are tabulated in Table III.

From the XRD results and scanning electron micrographs, it can be seen that both the particle size and the size distribution of the samples synthesized hydrothermally from a single precursor are a strong function of the base species used, whereas the phase composition and particle shape are not.

Fig. 3 shows the particle charge mobility plotted against pH measured using the Delsa 440 for the single-component sols of barium hydroxide and iron oxide (synthesized hydrothermally from barium nitrate and iron nitrate, respectively, under the standard synthesis conditions) as a function of base species used. It appears that the charge mobility behaviour and isoelectric point (IEP) of both the barium hydroxide and iron oxide sols are strongly dependent on the base species. It should be mentioned that the isoelectric point is the pH at which the zeta potential is zero and for oxides this point may be coincident with the point of zero charge (PZC), which is the pH at which the charge on the surface of the particles is zero. The point of zero charge for natural and synthetic iron oxide have been reported to occur at pH 4.8 and pH 8.6, respectively [15]; the average IEP pH value

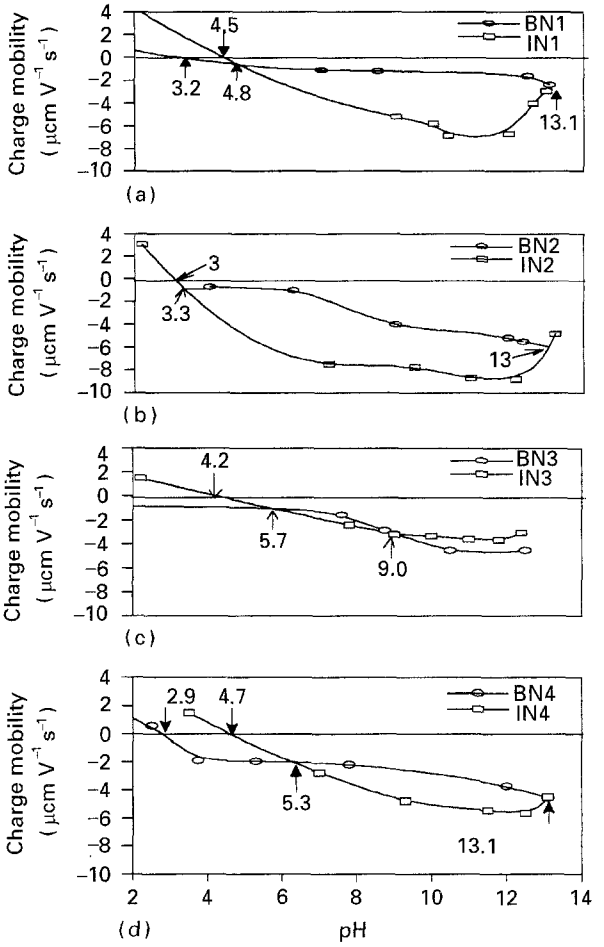

Figure 3 Particle surface charge mobility plotted against pH for barium hydroxide and iron oxide as a function of base species. (a) NaOH, (b) KOH, (c) NH_4OH, (d) $(C_2H_5)_4NOH$.

of 4.1 for iron oxide obtained in the current work coincides with the reported PZC value for natural iron oxide.

The variation in mobility behaviour and the IEP pH are related to the physicochemical characteristics of the electrical double layer (e.g. the extent and polarity of the Stern and diffuse layers) around the nucleated elementary sol particles of the sol, as shown by the schematic diagram in Fig. 4.

Generally, for aqueous sols of metal oxides, the preferential absorption of either hydrogen (H^+) or hydroxide (OH^-) ions is responsible for the net surface charge [16]; therefore they are known as potential determining ions. The extent and net polarity of the double layer is affected by the characteristics of the

TABLE III Particle shape, mean particle diameter (determined by SEM) and mean, modal and 95% confidence limits particle sizes (from Coulter LS 130) of the products from the hydrothermal processing of the iron nitrate under the standard synthesis conditions as a function of base species

Sample	Base	Shape of the particles	Mean diameter (μm) SEM	Mean size (μm) LS 130	Mode (μm) LS 130	95% Conf. limits (μm) LS 130
IN1	NaOH	Plate-like hexagonal	0.5	12.93	8.28	8.39–17.53
IN2	KOH	Plate-like hexagonal	0.4	12.28	13.05	10.78–13.78
IN3	NH_4OH	Plate-like hexagonal	0.4	5.03	3.33	4.10–5.96
IN4	$(C_2H_5)_4NOH$	Plate-like hexagonal	0.15	3.29	3.65	2.89–3.68

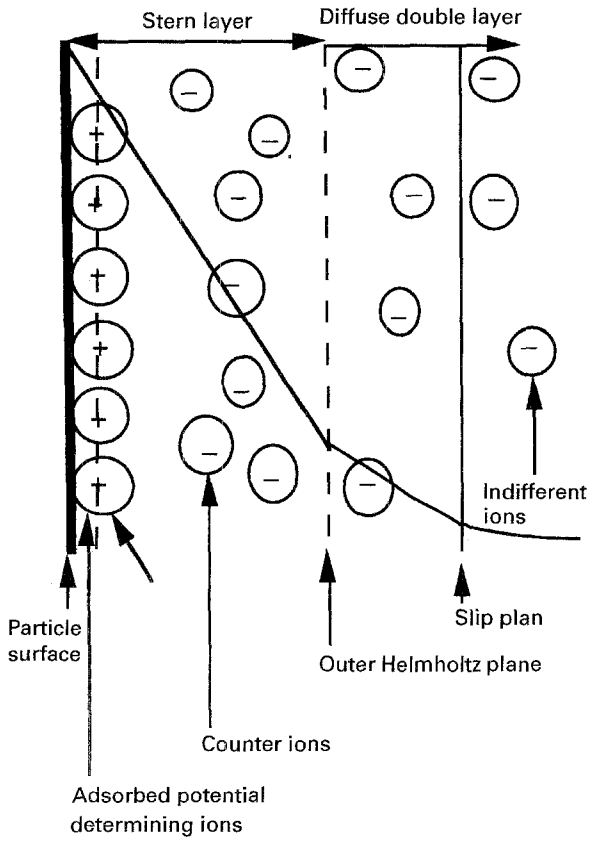

Figure 4 Schematic diagram of the double layer around the negatively charged particle.

interchangeable base-species anions and cations in and around the double layer. The balance between the thermal energy and electrostatic potential energy of the ions in solution (near the charged surface) controls the extent of the diffuse layer [16]. The double-layer characteristics can also be influenced by the concentration of pH/added ions and ionic size which controls the surface charge packing density in the Stern layer in contact with the particles.

At the experimental synthesis pH (around 12), both the barium hydroxide and iron oxide (synthesized with different base species) sol particles are charged negatively but with different magnitudes. The electrostatic potential difference between the barium hydroxide and the iron oxide particles decreases with increasing cation size in the order NaOH, KOH, $(C_2H_5)_4NOH$ and NH_4OH. Note that in NH_3 (aq), there are no NH_4OH molecules as such; rather the ammonia molecules are hydrogen bonded to water molecules, giving a low dissociation constant. Thus, it is assumed that the "NH_4 cation" is larger than the "$(C_2H_5)_4N$ cation".

The potential difference between the two sol species determines their tendency to coagulate into clusters; hence, the heterocoagulation will be greater when using NaOH or KOH than $(C_2H_5)_4NOH$ or NH_4OH. Therefore, the formation of barium hexaferrite will be easier. Note that for a given base, there is a pH range or value at which the heterocoagulation tendency is maximized, thus optimizing the yield of heterocoagulated sol particles. Hopefully, many will be of barium hexaferrite composition.

3.2. Hydrothermal processing of barium and iron nitrates in combination

Fig. 5 illustrates the powder X-ray diffraction patterns of products synthesized hydrothermally from a barium and iron nitrate mixture under the standard synthesis conditions as a function of base species. Analysis of these patterns confirms the formation of barium hexaferrite ($BaFe_{12}O_{19}$) for samples synthesized in the presence of NaOH or KOH, and mainly αFe_2O_3, and small proportions of $BaFe_{12}O_{19}$ and $BaFe_2O_4$ for samples synthesized in the presence of NH_4OH or $(C_2H_5)_4NOH$.

From the XRD results, it may be suggested tentatively that barium hexaferrite is being formed in three stages in the autoclave according to the following reactions, the intermediate phases of αFe_2O_3 and $BaFe_2O_4$ being formed first

$$2Fe(OH)_3 \rightarrow \alpha Fe_2O_3 + 3H_2O \quad (1)$$

$$\alpha Fe_2O_3 + Ba(OH)_2 \rightarrow BaFe_2O_4 + H_2O \quad (2)$$

$$BaFe_2O_4 + 5\alpha Fe_2O_3 \rightarrow BaFe_{12}O_{19} \quad (3)$$

The average size, d, thickness, t, and aspect ratio d/t, of the barium hexaferrite particles are given in Table IV as a function of base species.

Fig. 6 shows a scanning electron micrograph in which the uniform size of the hexagonal plate-like and uniform particles of barium hexaferrite particles

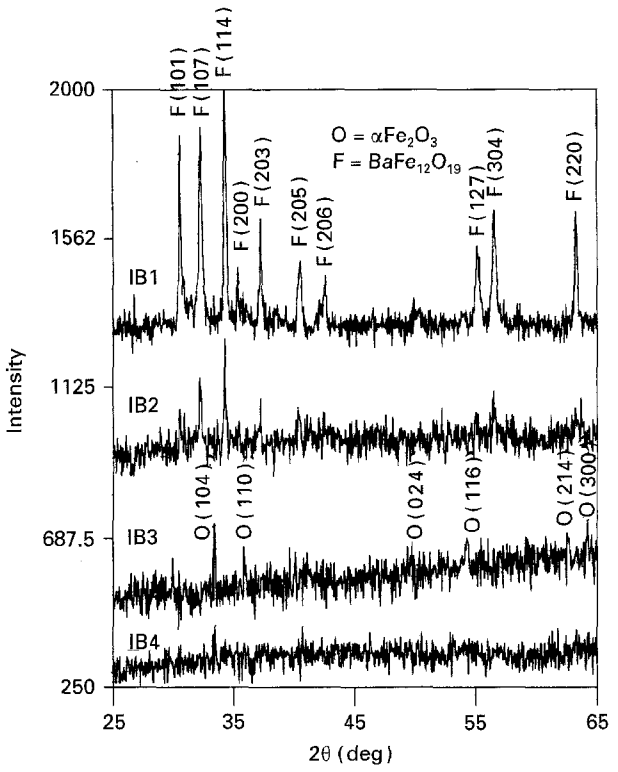

Figure 5 X-ray powder diffraction patterns of products synthesized hydrothermally from barium and iron nitrates under the standard synthesis conditions as a function of base species.

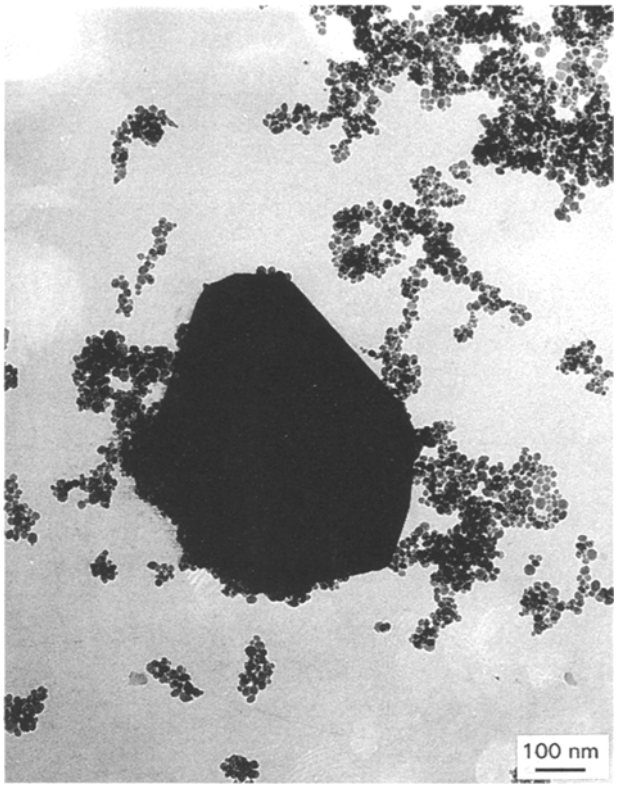

Figure 7 Transmission electron micrograph of products synthesized hydrothermally from a barium and iron nitrate mixture in the presence of $(C_2H_5)_4NOH$ under the standard synthesis conditions.

TABLE IV Average size, d, thickness, t, and aspect ratio, d/t, of barium hexaferrite particles synthesized hydrothermally from a barium and iron nitrate mixture under the standard synthesis conditions as a function of base species

Sample	Base	d (μm) SEM	t (μm) SEM	d/t SEM
IB1[a]	NaOH	1.2	0.28	4.2
IB2[a]	KOH	0.9	0.2	4.13
IB3[a]	NH_4OH	0.8	0.15	5.3
IB4[b]	$(C_2H_5)_4NOH$	0.9	0.06	15

[a] Measured from scanning electron micrographs.
[b] Measured from transmission electron micrographs.

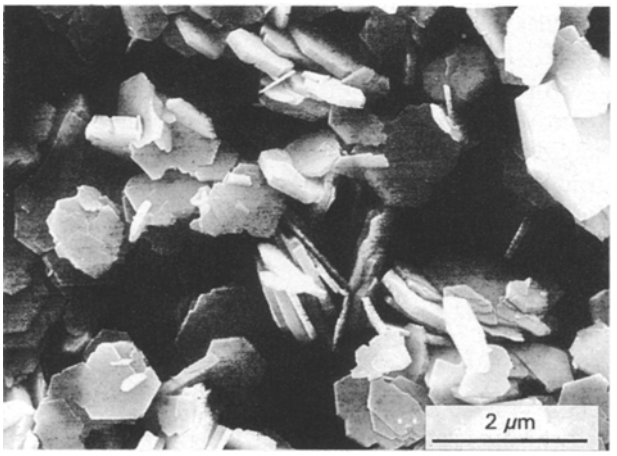

Figure 6 Scanning electron micrograph of barium hexaferrite synthesized hydrothermally from a barium and iron nitrate mixture in the presence of KOH under the standard synthesis conditions.

synthesized in the presence of KOH can be seen. In contrast, the transmission electron micrograph in Fig. 7 shows the sample synthesized in the presence of $(C_2H_5)_4NOH$ to consist almost entirely of ultrafine hexagonal particles of the intermediate phases (predominantly αFe_2O_3 according to the XRD results), whose sizes range from 10–20 nm. Note the presence of a relatively large particle of barium hexaferrite, whose size is about 0.5 μm. The average particle size of the barium hexaferrite synthesized in the presence of KOH is smaller than that synthesized in the presence of NaOH; this may be due to either an increase in the nucleation rate or a decrease in the growth rate or both. Although the KOH produced a relatively high sol solution pH of 13.80 compared with pH 13.5 when using NaOH, the effect on the charge mobility behaviour is different and the K^+ ion (0.133 nm) being larger than the Na^+ ion 0.097 nm), is producing a steric hindrance effect on the formation and especially the growth of the barium hexaferrite particles. Fig. 5 and the Table IV data tend to support the idea of a steric hindrance effect on the formation and growth of barium hexaferrite particles.

The DTA traces of the above mentioned samples likewise showed different behaviour as a function of base species; the salient results are tabulated in Table V. It appears that the thermal behaviour of the samples and the formation temperature of barium hexaferrite are strong functions of the base species. According to the XRD results, the initial phase composition of sample IB4 consists mainly of αFe_2O_3 and small amounts of $BaFe_{12}O_{19}$ and $BaFe_2O_4$. After calcination at 850 °C for 1 h, the sample was predominantly

TABLE V DTA traces for the products synthesized hydrothermally from a barium and iron nitrate mixture under the standard synthesis conditions as a function of base species

Sample	Base	Endothermic peak (°C)	Exothermic peak (°C)	Probable explanation of peak
IB1	NaOH	~ 100	–	Loss of water
IB2	KOH	~ 100		Loss of water
			~ 287	Volatilization of some unreacted phase
IB3	NH_4OH	~ 100		Loss of water
			~ 287	Volatilization of some unreacted phase
			1172	Formation of $BaFe_{12}O_{19}$
IB4	$(C_2H_5)_4NOH$	~ 100		Loss of water
			287	Volatilization of some unreacted phase
			660	Formation of $BaFe_2O_4$
			794	Formation of $BaFe_{12}O_{19}$

$BaFe_{12}O_{19}$ with a small amount of the $BaFe_2O_4$ and αFe_2O_3 present. In contrast, however, no significant change in the phase composition of sample IB3 was observed after calcination under the same conditions.

The magnetic properties of the products synthesized hydrothermally from mixtures of barium and iron nitrate are also altered significantly as a function of the base species. Fig. 8 shows the magnetization plotted against applied field for the above samples as a function of base species; their magnetic properties are tabulated in Table VI. The samples synthesized in the presence of NH_4OH or $(C_2H_5)_4NOH$ exhibit negligible magnetization owing to the small amount of magnetic phase ($BaFe_{12}O_{19}$) present (as shown earlier in Fig. 5).

The saturation magnetization, σ_s (measured at 1.4 T) (14 kOe) and remanence, B_r, of the samples are shown in Fig. 9 as a function of sol solution pH (measured after synthesis). These parameters increase with increasing pH (due to a concomitant increase in the proportion of magnetic phase present) and go through a maximum. The decrease in σ_s and B_r at a pH close to 13 is attributed to the decrease in the electrostatic potential difference between the barium hydroxide and iron oxide sol particles and hence, their degree of heterocoagulation (as considered in Fig. 3). The saturation magnetization of strontium hexaferrite (synthesized hydrothermally from nitrate precursors in the presence of NaOH) as a function of NaOH concentration (i.e. molar ratio of OH^-/NO_3^-) exhibited similar behaviour to that shown in Fig. 10 [17].

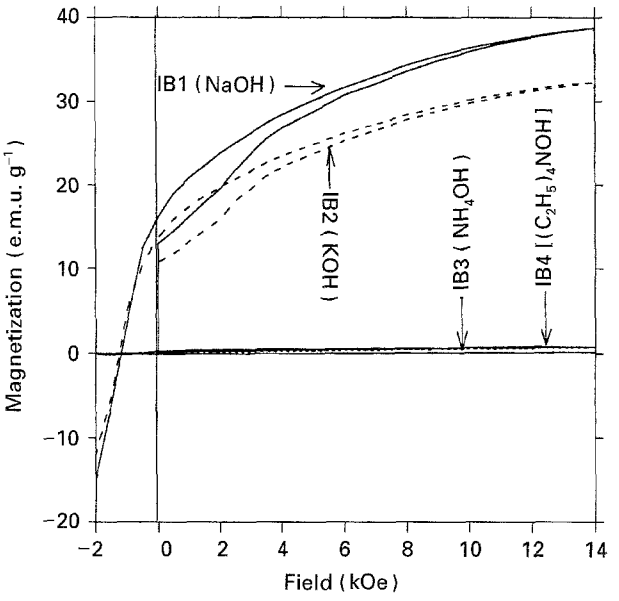

Figure 8 Magnetization versus applied field for products synthesized hydrothermally from a mixture of barium and iron nitrate under the standard synthesis conditions as a function of base species.

4. Conclusion

The hydrothermal synthesis of barium hexaferrite from nitrate precursors under specified synthesis conditions using different base species has been investigated.

Analysis of the results confirms that the presence of different base species can alter the course of the precipitation from solution and inhibit or aid the

TABLE VI Intrinsic coercivity $_iH_c$, remanence, B_r, and saturation magnetisation, σ_s, of products synthesized hydrothermally from a mixture of barium and iron nitrate under the standard synthesis conditions as a function of base species

Sample	Base	$_iH_c$ (kA m^{-1}) (kOe)	B_r (mT) (e.m.u. g^{-1})	σ_s (mT) (e.m.u. g^{-1}) at (14 kOe) 1.4 T
IB1	NaOH	94.57 (1.18)	107.43 (16.13)	258.47 (38.81)
IB2	KOH	99.42 (1.24)	90.44 (13.58)	215.19 (32.31)
IB3	NH_4OH	38.29 (0.48)	1.73 (0.26)	5.26 (0.79)
IB4	$(C_2H_5)_4NOH$	79.6 (1.0)	2.06 (0.31)	8.00 (1.2)

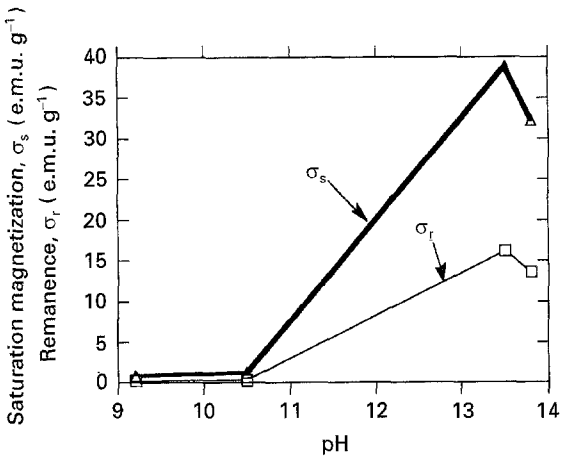

Figure 9 Saturation magnetization and remanence of the samples as a function of post-synthesis sol solution pH.

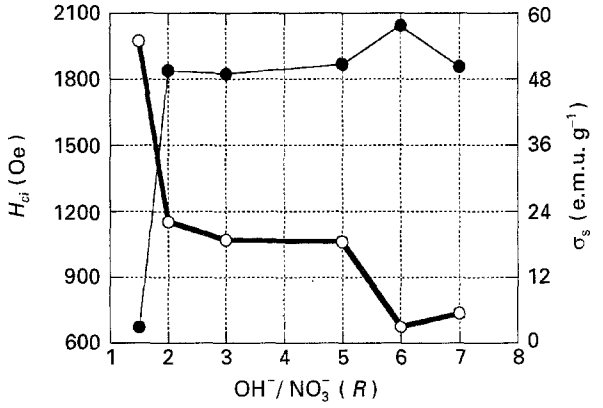

Figure 10 (○) Intrinsic coercivity, H_{ci}, and (●) saturation magnetization, σ_s (measured at 1.4 T (14 kOe)), of strontium hexaferrite as a function of alkali molar ratio [17].

formation of barium hexaferrite; i.e. the percentage of barium hexaferrite decreased from 100 wt % to about 10 wt % when NaOH was replaced with NH_4OH.

The pH of the sol solution in the autoclave (which is related to the base species) plays an important role in this process. The effect of the pH on the phase composition, particle size and size distribution, thermal behaviour, agglomeration behaviour and magnetic properties of the samples synthesized from composite precursors (barium and iron nitrates simultaneously) is more marked than that on products synthesized from a single precursor.

For samples synthesized from a barium and iron nitrate mixture (samples IB1, IB2, IB3 and IB4), the barium hexaferrite particle size and saturation magnetization, as well as the amount formed increases with increasing pH up to about pH 13.25, while the coercivity and formation temperature of barium hexaferrite decrease. However, when the pH increases above 13.25, the converse is true.

Analysis of the results has also shown that both the surface charge density of the barium hydroxide and iron oxide particles and the electrostatic potential between them, and hence, their tendency to form barium hexaferrite, are strong functions of the base species and the sol solution pH. It seems that, at particular pH values (e.g. at pH 12), except for the pH values where the charge mobilities are identical, the electrostatic potential between the barium hydroxide and iron oxide particles is influenced by the base species cation size and decreases with increasing cation size.

It is thus suggested that any change in the surface charge characteristics of the particles (of the above-mentioned compounds) is likely to result in changes in the phase composition, thermal behaviour, particle morphology, particle agglomeration behaviour, and hence, magnetic properties of the samples.

Acknowledgements

The authors thank the members of the Applied Alloy Chemistry Group (School of Metallurgy and Materials) and the Ceramic Group (IRC/School of Metallurgy and Materials) for their help and cooperation. The provision of facilities by Professor J. F. Knott FRS FEng (Metallurgy and Materials) and Professor M. H. Loretto (IRC) is acknowledged. The financial support of A. A. by the Iranian government during his PhD studentship is also gratefully acknowledged.

References

1. H. SAKAI, K. HANAWA and K. AOYAGI, *IEEE Trans. Mag.* **28** (1992) 3355.
2. V. V. PANKOV, M. PERNET , P. GERMI and P. MOLLARD, *J. Mag. Mag. Mater.* **120** (1993) 69.
3. F. LICCI and T. BESAGNI, *IEEE Trans. Mag.* **MAG 20** (1984) 1639.
4. K. HIGUCHI, S. NAKA and S. I. HIRANO, *Adv. Ceram. Mater.* **1** (1986) 104.
5. U. MEISEN and A. EILING, *IEEE Trans. Mag.* **26** (1990) 21.
6. V. K. SANKARANARAYANAN, Q. A. PANKHURST, D. P. E. DICKSON and C. E. JOHNSON, *J. Mag. Mag. Mater.* **120** (1993) 73.
7. M. KIYAMA, *Bull. Chem. Soc. Jpn* **49** (1976) 1855.
8. D. BARB, L. DIAMANDESCU, A. RUSI, D. MIHALLA, M. MORARIU and V. TEODORESCU, *J. Mater. Sci.* **21** (1986) 1118.
9. E. SADA, H. KUMAZAWA and H. M. CHO, *Ind. Eng. Chem. Res.* **30** (1991) 1319.
10. M. L. WANG and Z. W. SHIH, *J. Crystal Growth* **116** (1992) 483.
11. H. KUMAZAWA, H. M. CHO and E. SADA, *J. Mater. Sci.* **28** (1993) 5247.
12. T. TAKADA, Y. IKEDA, H. YOSHINAGA and Y. BANDO, in "Proceedings of the International Conference on Ferrites", Japan (1970) pp. 275–8.
13. C. H. LIN, W. SHIH, T. S. CHIN, M. L. WANG and Y. C. YU, *IEEE Trans. Mag.* **MAG 26** (1990) 15.
14. M. YOSHIMURA, N. KUODERA, T. NOMA and S. SOMIYA, *J. Ceram. Soc. Jpn* **97** (1989) 16.
15. R. J. HUNTER, "Zeta Potential in Colloid Science" (Academic Press, London, 1981).
16. C. W. TURNER, *Ceram. Bull.* **70** (1991) 1487.
17. A. ATAIE, I. R. HARRIS and C. B. PONTON, *J. Mater. Sci.* **30** (1995) 1429.

Received 22 December 1994
and accepted 15 March 1995